



HAL
open science

Multicopter Sizing Methodology with Flight Time Estimation

Marcin Biczyski, Rabia Sehab, James Whidborne, Guillaume Krebs, Patrick Luk

► **To cite this version:**

Marcin Biczyski, Rabia Sehab, James Whidborne, Guillaume Krebs, Patrick Luk. Multicopter Sizing Methodology with Flight Time Estimation. *Journal of Advanced Transportation*, 2020, 2020, pp.9689604. 10.1155/2020/9689604. hal-02504788

HAL Id: hal-02504788

<https://centralesupelec.hal.science/hal-02504788>

Submitted on 11 Mar 2020

HAL is a multi-disciplinary open access archive for the deposit and dissemination of scientific research documents, whether they are published or not. The documents may come from teaching and research institutions in France or abroad, or from public or private research centers.

L'archive ouverte pluridisciplinaire **HAL**, est destinée au dépôt et à la diffusion de documents scientifiques de niveau recherche, publiés ou non, émanant des établissements d'enseignement et de recherche français ou étrangers, des laboratoires publics ou privés.

Journal of Advanced Transportation

Multicopter Sizing Methodology with Flight Time Estimation

Marcin Biczyski¹, Rabia Sehab¹, James F. Whidborne², Guillaume Krebs³ and Patrick Luk⁴

¹On-board Energies and Systems Division, ESTACA Campus West, 53000 Laval, France

²Centre for Aeronautics, Cranfield University, MK43 0AL Cranfield, UK

³Pôle "Systèmes" ECo2, GeePs - CentraleSupélec, 91192 Gif sur Yvette, France

⁴Centre for Thermal Energy Systems and Materials, Cranfield University, MK43 0AL Cranfield, UK

Correspondence should be addressed to Marcin Biczyski: marcin.biczyski@estaca.fr

Abstract

This paper addresses the need for sizing of rotors for multicopter vehicle applications such as personal air transport, delivery, surveillance and photography. A methodology for the propeller and motor selection is developed and augmented with flight time estimation capabilities. Being multicopter-specific it makes use of the platform's simplicity to rapidly provide a set of off-the-shelf components ready to be used in the vehicle. Use of operating points makes the comparison process fast, precise and tailored to specific application. The method is easily implemented in software to provide an automated tool. Furthermore, clearly defined input and output parameters make it also usable as a module in other multicriteria optimisation algorithms. The new methodology is validated through comparison with consumer-grade drone and the calculated results are compliant with manufacturer's specification in terms of maximum hover time.

Keywords— BLDC, Multicopter, PAV, Propeller, Sizing, UAV

1 Introduction

In recent years Unmanned Aerial Vehicles (UAVs), have become a popular solution for a variety of civil and military applications including surveillance, photo- and videography and land surveying. The versatility of these systems has even found them in many non-standard purposes such as automated package delivery or Personal Air Vehicles (PAVs). Multicopter UAV platforms have gained particular attention due to their Vertical Take Off and Landing (VTOL) capabilities as well as their simple construction and control. Of paramount importance is safety and reliability, especially when it comes to autonomous solutions, and so the enterprise market offers complete, closed drone solutions at different size/weight points. These are simple-to-use systems with high degree of user support and good performance for most applications. However, the mechanical simplicity of the platform means that customized and open solutions should be available for specialized applications. Furthermore, the main limitation of multicopter systems is their flight time, mostly due to battery

38 weight and energy storage constraints. Therefore, a set of tools needs to be created that can aid the
39 design of customized solutions that can be specifically tailored for a particular application. Thus
40 there is a need for a methodology to automatically select the best consumer-grade components to
41 build a custom solution at a given weight and performance level.

42 There are few methodologies in the open literature for this purpose; and none lead directly to a
43 “bill-of-materials” level solution. The most popular approach to obtaining a “flyable” configuration
44 seems to be to test various *motor + propeller* combinations and choose one that suits the application
45 ([1]). Although popular with hobbyists, the method has little value in the commercial or research
46 environment due to high cost (purchase of components), time requirement and the need for specialized
47 equipment (thrust stand, dynamometer). This method provides the most accurate results, but the
48 number of combinations needed to be tested increases geometrically with each added component.
49 This process can be significantly sped up using calculators such as Drive Calculator [2] and eCalc [3],
50 which incorporate some of the data in their databases, but still the selection needs to be performed
51 manually.

52 Although not solving the problem completely, there are several methods that help with the
53 preliminary multirotor design. Basset et al. [4] present past and current efforts to develop UAV
54 pre-sizing methodologies. They focus on conceptual, as well as numerical aspects of the vehicle.
55 Due to the confidential nature of the projects, the paper does not go into much detail of the inner
56 working of the methodologies. However, most of them share a trait of being as general as possible
57 in order to make them applicable to every configuration, which is not desired when dealing with
58 an already chosen topology, such as multirotor, due to possible oversimplification and loss of
59 optimisation opportunities.

60 Multirotor-specific methodologies were developed by Gatti and Giulietti [5], Gatti [6] and
61 Kim et al. [7]. They all use statistical methods to estimate relations between different components
62 of the propulsion chain. The first two use analytical methods from the area of aerospace to
63 calculate take-off weight based on mission requirements, and the last manages to simplify the drone
64 propulsion model to one equation that allows to obtain power or thrust generated. Unfortunately,
65 these approaches provide too little data to properly size the components, and in some cases even
66 require the data of a selected component to work. Therefore, while useful for calculating the target
67 multirotor weight for the application, they cannot be used for the component selection process.

68 This paper presents a method for sizing of the multirotor propulsion system through the
69 selection of propeller and motor. Furthermore, the method provides the necessary data for the
70 selection of the Electronic Speed Controller (ESC) and battery. Additionally, it gives a way of
71 comparing different configurations through estimation of flight time by modelling battery discharge
72 at constant power requirement. The key point of the methodology is the fact that it works on real
73 components (propellers and motors) increasing the precision of the estimation. Another feature is
74 the ability for the selection process to be automated making it an useful module for use in novel
75 optimisation algorithms. It should be noted that the resultant configuration is based on estimations,
76 assumptions and inaccurate data, and therefore not optimal, so the methodology results should be
77 treated only as a *good first guess*.

78 The paper is structured as follows; Section 2 details all the elements of the multirotor
79 propulsion chain and their interaction; Section 3 describes the methodology based on the inverted
80 model from the previous section; Section 4 presents example results for a small drone such as DJI
81 Phantom 4 V2.0 and extends the findings onto Personal Air Vehicles; finally, Section 5 concludes
82 the paper and highlights the most important outcomes.

83 2 Multirotor propulsion chain

84 Multirotors as a category of flying vehicles cover a lot of variants differing not only in the number
85 of rotors, but also their placement. Currently, the most popular configuration seems to be *quad X*
86 with 4 rotors placed diagonally from the centre, as shown in Figure 1. One of the characteristic
87 properties of most multirotors is their symmetry and the fact that every arm is the same, except for
88 rotor spinning direction. This makes it easy to analyse the propulsion system for the general case by
89 analysing only one arm (one propulsion chain). The Flight Controller (FC) is responsible for control
90 strategy for the whole platform and preparing a set point for each arm, but it does not participate in
91 the propulsion chain as such.



Figure 1: Multirotor in *quad X* configuration with visible components of the propulsion chain. (i) Flight Controller, (ii) ESC (under arm), (iii) BLDC Motor, (iv) propeller, (v) battery connector.

92 In most cases Brushless DC (BLDC) motors are used for multirotor propulsion, but sometimes,
93 usually for toys under 100 g, DC motors are also used. This paper focuses only on BLDC, however
94 most concepts shown apply to both types. Brushless motors do not have physical brushes, so they
95 require Electronic Speed Controllers (ESC) to achieve electronic commutation. Therefore the main
96 components of the propulsion chain are identified to be: *propeller*, *motor*, *ESC* and *battery*. A
97 schematic of the propulsion model of a multirotor is shown in Figure 2. It can be seen that there is
98 one input of a set point (given by FC) and one output, namely the thrust generated by the propeller.
99 Therefore, the propulsion chain can be identified as an open-loop Single Input Single Output (SISO)
100 system, which makes it relatively easy to size components one at a time. In the next part of this
101 section, each component will be described in detail.

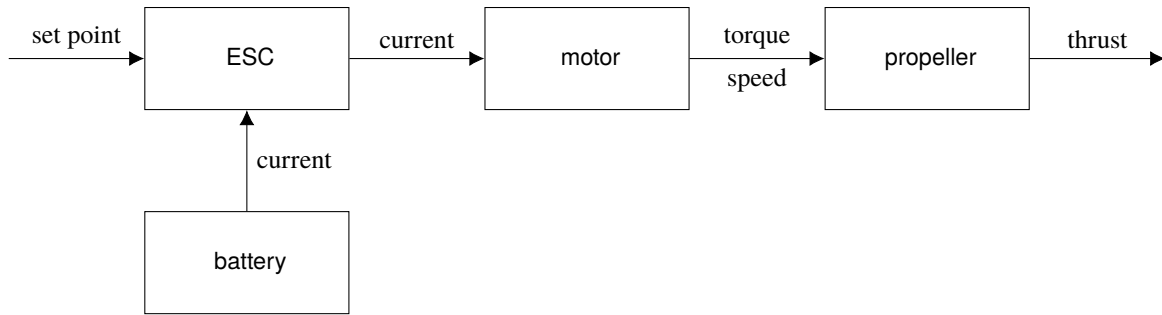


Figure 2: Multirotor propulsion chain diagram.

102 2.1 Propeller

103 Aircraft propellers are characterized by 3 main parameters: diameter, pitch and the number of blades.
 104 Generally the higher they are, the higher thrust is generated, but also higher torque is exerted on the
 105 motor. However, long, slowly-spinning, 2-bladed propellers are known to be more aerodynamically
 106 efficient than small, fast-spinning, multi-bladed ones. Propeller characteristics are mainly a function
 107 of its rotational speed and the speed of incoming air. However, if we consider air density to be
 108 constant and the air to be static (drone flight speed of 0), the thrust, torque and power depend only on
 109 propeller speed. Additionally, there are secondary parameters such as mass and geometry template
 110 expressed as manufacturing series (e.g. Multirotor, Slow Flyer, Carbon, etc.).

111 2.2 Motor

112 In a multirotor, the motor's main objective is to drive the propeller reliably and with high acceleration,
 113 so the speed can be changed quickly. The main limitations of a BLDC motor are in terms of speed
 114 and current. Maximum current is often stated by the manufacturer and maximum speed in no-load
 115 conditions ω_0 can be calculated from the KV parameter multiplied by the applied voltage V :

$$116 \quad \omega_0 = KV \times V. \quad (1)$$

117 With a constant voltage, when current is applied, the motor starts exerting torque on the
 118 shaft accelerating it until its torque equals the load torque, assuming the mechanical losses are
 119 neglected. At low speed - far from the motor constraints, it is assumed that the relation between
 120 motor torque and current is constant and expressed with motor torque constant (K_T). Therefore, the
 121 applied current is transformed into the torque based on the motor characteristic, then the torque is
 122 transformed into speed based on the propeller torque-speed characteristic, and finally the speed is
 123 transformed into thrust using the propeller thrust-speed characteristic. This sequence makes the
 124 propulsion chain easy to calculate analytically as a SISO system.

125 2.3 Electronic Speed Controller

126 Although Electronic Speed Controllers (ESCs) serve a very important purpose in the real-life
 127 multirotor, in the propulsion chain model it has very little importance. In the model, its function is
 128 reduced to transferring current from the battery to the motor under constant voltage. However, when

129 designing a multirotor, ESC still needs to be sized according to the maximum current flowing to the
130 motor.

131 2.4 Battery

132 When it comes to lightweight aerial vehicles, Lithium Polymer (LiPo) batteries currently dominate
133 the market due to their high energy density and high current discharge capabilities [6], [8]. These
134 batteries are composed of several cells connected in series (rarely in parallel). Cell voltage changes
135 according to the state of charge with 4.2 V being at 100%, 3.85 V at 50% and 3.7 V (nominal)
136 at 20%. However, discharging a LiPo cell under 3 V leads to permanent damage to the battery.
137 Therefore, it is recommended to only discharge the batteries to about 20%, which grants a Depth of
138 Discharge (DoD) of 80%. The cells can be connected in series or in parallel, denoted by S or P
139 respectively, so for example, $4S1P$ is a 4 cell battery with 14.8 V nominal voltage. Additionally,
140 the batteries are characterized by their capacity in mAh and a C-rating (r_C), which specifies the
141 maximum current that can be drawn continuously, for example $35C \times 5.2Ah = 182A$ (the unit being
142 C and not Coulomb). It is evident that maximum discharge current is not dependent on battery
143 capacity.

144 3 Sizing methodology

145 By inverting the propulsion system model developed in the previous section, a new model can
146 be obtained allowing to estimate battery voltage based on thrust generated, as shown in Figure
147 3. This allows for an iterative approach in order to determine the time required to deplete the
148 battery at constant power draw, which effectively serves as a flight time estimate. Thus, two distinct
149 sub-systems can be distinguished in the system model: the actuating system and the power system.
150 This manifests itself in the sizing methodology, which is also divided into two parts. Figure 4 shows
151 a simplified view of the methodology.. Although it is based on the diagram in Figure 3, it also shows
152 the separation between battery sizing and battery simulation (flight time simulation).

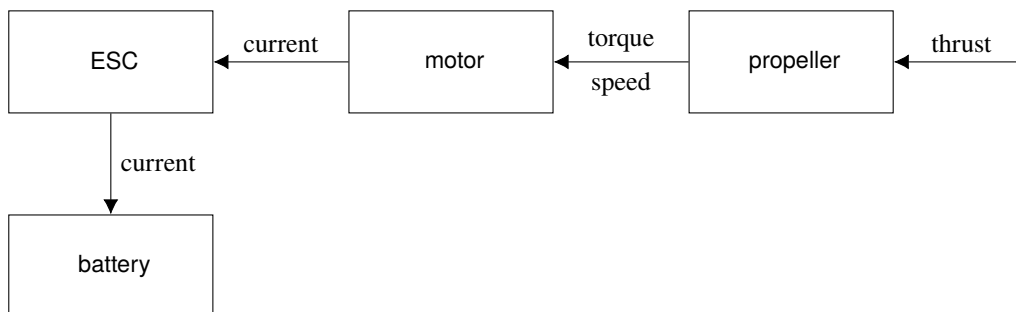


Figure 3: Inverted multirotor propulsion chain diagram.

153 3.1 Actuating system

154 The actuating system provides the thrust propulsion to the vehicle and consists of the propeller, the
155 motor, an ESC to control the motor and a battery to power the motor. The propeller sizing and

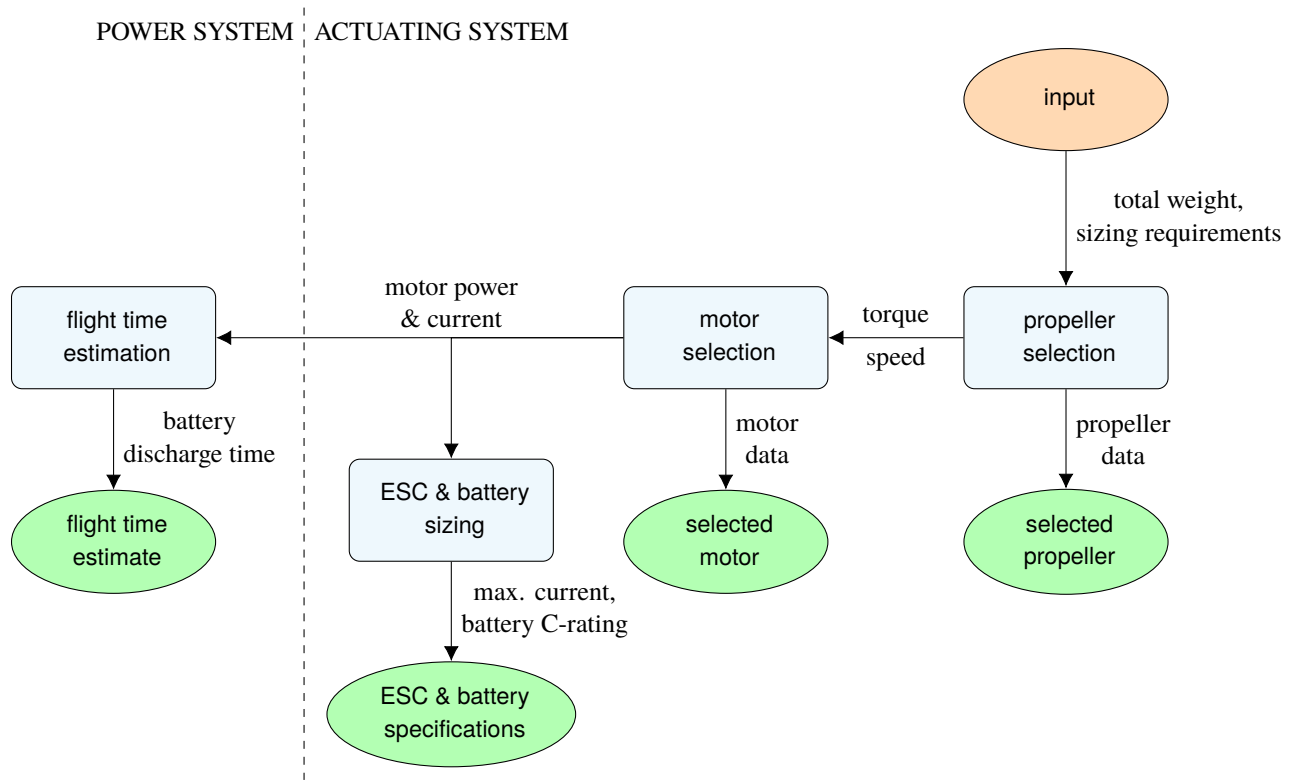


Figure 4: Simplified sizing methodology flowchart with division into two sub-systems.

156 selection is performed first, the motor sizing being dependent on the propeller properties. Finally,
 157 specifications for the ESC and the battery are produced.

158 The propulsion system model used here is only applicable in static conditions and at
 159 constant speed. Modelling a multirotor in flight is much more complicated due to the presence of
 160 aerodynamic effects such as variable angle of attack, reduction of thrust coefficient with advance
 161 ratio and additional frame drag. However, an approximation of the required performance for full
 162 controllability in flight is made using the model only in static conditions of operation. It uses a state
 163 of equilibrium achieved at hover (in no-wind conditions), where thrust generated by the propellers is
 164 equal to the multirotor's weight. This thrust can be multiplied by a constant thrust-to-weight ratio
 165 to achieve a value of static thrust that guarantees specific performance in the air depending on the
 166 application. This approach appears imprecise, however, during the years of use of similar methods
 167 in the community of radio controlled aircraft modellers, the values of thrust-to-weight ratio required
 168 for different applications have been validated with many test flights. A quick summary of typical
 169 values can be found in Table 1, which is based on [9] and [10]. Additionally, in static conditions
 170 there is no influence of rotor inertia on motor performance, so the propeller and motor selection can
 171 be decoupled, further simplifying the process.

Table 1: Typical applications for multirotors of different thrust-to-weight ratios.

Thrust-to-weight ratio	Application
2	slow flight (minimum)
3	payload transport; photography
4	surveillance
5+	aerobatics; high-speed video
7+	racing

172 3.1.1 Propeller sizing and selection

173 The propeller sizing and selection process starts by defining a propeller database represented as a
174 set of available propellers

$$175 \mathcal{P} := \{\mathbf{p}_i : i = 1 \dots n_p\} \quad (2)$$

176 where the i th propeller \mathbf{p}_i is defined by the pair

$$177 \mathbf{p}_i := (\mathbf{f}_{pi}, \mathbf{g}_{pi}) \quad (3)$$

178 where \mathbf{f}_{pi} denotes the i th propeller performance, which will be defined later, and \mathbf{g}_{pi} denotes its
179 physical properties expressed as a 4-tuple

$$180 \mathbf{g}_{pi} := (d_i, \theta_{pi}, m_{pi}, s_{ni}) \quad (4)$$

181 where d_i is the i th propeller diameter, θ_{pi} is its pitch angle, m_{pi} is its mass and s_{ni} is a discrete
182 parameter representing the propeller series name. The propeller set \mathcal{P} is then filtered to obtain a set
183 of propellers $\mathcal{P}_p \subseteq \mathcal{P}$ that satisfy a requirement 4-tuple

$$184 \mathbf{g}_{pr} = (d_{\min}, d_{\max}, m_{p_{\max}}, \mathcal{S}_{nr}) \quad (5)$$

185 where d_{\min} is the minimum diameter, d_{\max} is the maximum diameter, $m_{p_{\max}}$ is the maximum mass,
186 and \mathcal{S}_{nr} is a set of preferred series names

$$187 \mathcal{S}_{nr} := \{s_{nk} : k = 1 \dots n_s\}. \quad (6)$$

188 Thus

$$189 \mathcal{P}_p = \{\mathbf{p}_i : d_i \in [d_{\min}, d_{\max}], m_{pi} \in (0, m_{p_{\max}}], s_{ni} \in \mathcal{S}_{nr}\}. \quad (7)$$

190 This helps save time when evaluating the performance data and calculating operating points that is
191 done next.

192 The performance of the i th propeller \mathbf{f}_{pi} is denoted as a triplet of bijective mappings

$$193 \mathbf{f}_{pi} := (\omega \mapsto T(\omega), \omega \mapsto \tau(\omega), \omega \mapsto P_p(\omega)) \quad (8)$$

194 where ω is the rotor speed, T is the thrust, τ is the torque and P_p is the propeller power. Let
195 $T_r^{(k)}$ denote a required thrust. For each $\mathbf{p}_i \in \mathcal{P}_p$, we determine a set of n_o operating points
196 $o_{pi} = \{o_{pi}^{(k)} : k = 1 \dots n_o\}$ where

$$197 o_{pi}^{(k)} := (T_i^{(k)}, \omega_i^{(k)}, \tau_i^{(k)}, P_{pi}^{(k)}) \quad (9)$$

198 and where

$$199 \quad T_i^{(k)} = T_r^{(k)}, \quad (10)$$

$$200 \quad \omega_i^{(k)} = T^{-1}(T_r^{(k)}), \quad (11)$$

$$201 \quad \tau_i^{(k)} = \tau(\omega_i^{(k)}), \quad (12)$$

$$202 \quad P_{pi}^{(k)} = P_p(\omega_i^{(k)}). \quad (13)$$

203 An example of the mapping triplets for two propellers is shown in Figure 5 along with an illustration
 204 of obtaining o_{pi} from T_r .

205 Usually $n_o = 2$ operating points are calculated: the operating point at hover $o_{pi}^{(1)}$, and the Wide
 206 Open Throttle (WOT) operating point $o_{pi}^{(2)}$. These signify the lower and upper boundaries of the
 207 flight performance respectively. A third operating point ($k = 3$) can also be defined that corresponds
 208 to the propeller limit speed designated by the manufacturer; this can be used for checking the
 209 feasibility of the other operating points. The thrust requirements, $T_r^{(1)}$ for the hover condition and
 210 $T_r^{(2)}$ for the WOT condition, can be calculated from

$$211 \quad T_r^{(1)} = \frac{W_{\text{total}}}{n_{\text{rot}}}, \quad (14)$$

$$212 \quad T_r^{(2)} = r_T \times T_r^{(1)} \quad (15)$$

213 where W_{total} is the estimated total weight of the multirotor, n_{rot} is the number of rotors and r_T is the
 214 thrust-to-weight ratio.

215 In practice, due to the fact that the propeller characteristics mappings defined by (8) are often
 216 given in the form of sample points, interpolation must be used for the calculations. This introduces
 217 errors. Therefore, although in theory $P_p = \tau\omega$, often in practice (dependence on k removed for
 218 notational simplicity)

$$219 \quad P_{pi} \neq \tau_i\omega_i, \quad (16)$$

220 hence an average of those two values is taken

$$221 \quad P_{pi_{\text{avg}}} = \frac{1}{2}(P_{pi} + \tau_i\omega_i). \quad (17)$$

222 To choose the propeller, various selection criteria are available. If $n_o > 1$ then determining the
 223 minimum power solution is a multiobjective problem, and some user interaction is then helpful in
 224 making the selection. However, it is often possible to reduce the problem to the simplest case for
 225 $n_o = 1$, where the lowest power at hover operating point can be computed as follows

$$226 \quad \mathbf{p}_{\text{selected}} := \arg \min_{\mathbf{p}_i \in \mathcal{P}_p} P_{pi_{\text{avg}}}^{(1)}. \quad (18)$$

227 3.1.2 Motor sizing and selection

228 In a similar manner as for the propeller, let \mathcal{M} be the set of available motors

$$229 \quad \mathcal{M} := \{\mathbf{m}_j = (\mathbf{f}_{mj}, \mathbf{g}_{mj}) : j = 1 \dots n_m\} \quad (19)$$

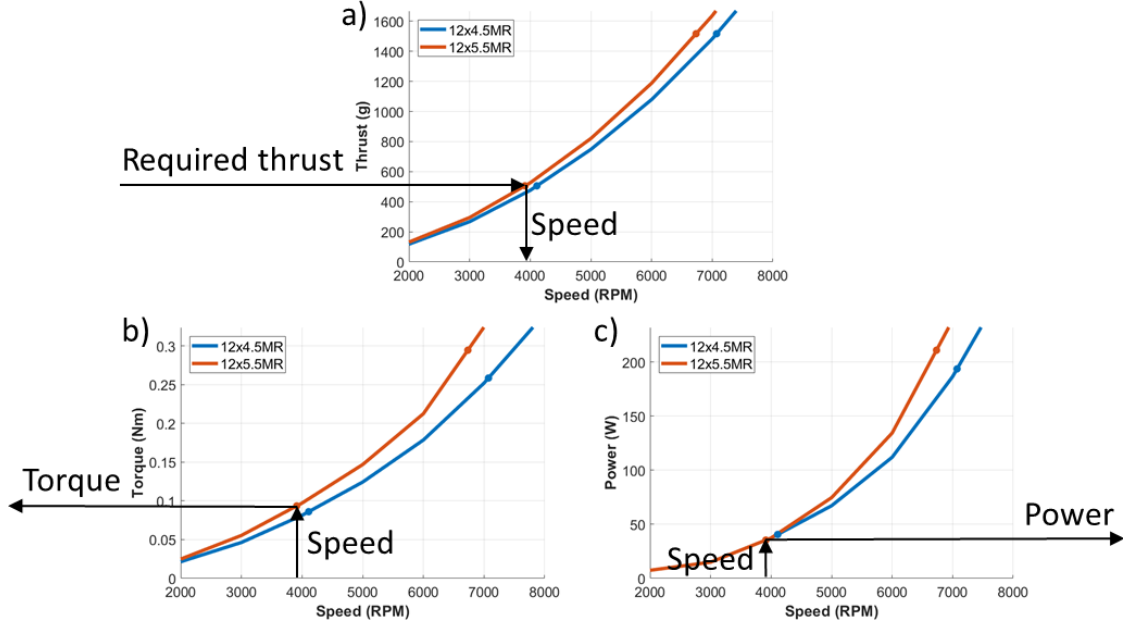


Figure 5: Example of obtaining a propeller operating point based on required thrust. *a)* Obtaining speed from required thrust. *b)* Obtaining torque from speed calculated in *a)*. *c)* Obtaining power from speed calculated in *a)*.

230 where \mathbf{f}_{mj} is the motor model described by the triplet of mappings

$$231 \quad \mathbf{f}_{mj} := (I \mapsto P_m(I), I \mapsto P_e(I), (P_m, P_e) \mapsto \eta(P_m, P_e)) \quad (20)$$

232 where I is the current, P_m is the mechanical power, P_e is the electrical power, η is the efficiency and
 233 where \mathbf{g}_{mj} denotes the motor properties expressed as a pair

$$234 \quad \mathbf{g}_{mj} := (I_{\max_j}, \omega_{0j}, m_{mj}) \quad (21)$$

235 where I_{\max_j} is the maximum allowable i th motor current, ω_{0j} is its maximum no-load speed and
 236 m_m is its mass.

237 Unlike the process for the propeller selection, the performances of the motors must be
 238 evaluated first. The required motor power is set to be $P_r = P_{p_{\text{selected}}}^{(k)}$. Then for each $\mathbf{m}_j \in \mathcal{M}$, we
 239 determine n_o motor operating point triplets

$$240 \quad \mathbf{o}_{mj}^{(k)} := (I_j^{(k)}, P_{ej}^{(k)}, \eta_j^{(k)}) \quad (22)$$

241 where (dependence on k removed for simplicity)

$$242 \quad I_j = P_m^{-1}(P_r), \quad (23)$$

$$243 \quad P_{ej} = P_e(I_j), \quad (24)$$

$$244 \quad \eta_j = \eta(P_r, P_{ej}). \quad (25)$$

245 It should be noted that the mapping $I \mapsto P_m(I)$ is not bijective in terms of motor characteristics,
 246 because at high current values most of the energy is dissipated as heat. However, considering the

247 domain only up to the maximum current specified by manufacturer, the function is almost always
 248 monotonic. Therefore, in practice, over the domain $[0; I_{\max_j}]$ the inverse of power function P_m^{-1} can
 249 almost always be evaluated.

250 Knowledge of o_{mj} for all $\mathbf{m}_j \in \mathcal{M}$ allows for filtering of the motor set in regards to maximum
 251 current, speed and mass, thus obtaining $\mathcal{M}_p \subseteq \mathcal{M}$ that satisfies maximum current requirement on
 252 each motor $I_j \leq I_{\max_j}$ and a requirement pair

$$253 \quad \mathbf{g}_{mr} = (\omega_{\max}, m_{m_{\max}}) \quad (26)$$

254 where $\omega_{\max} = \omega_{\text{selected}}^{(2)}$ is the propeller speed at WOT and $m_{m_{\max}}$ is the maximum motor mass.
 255 Thus

$$256 \quad \mathcal{M}_p = \{\mathbf{m}_j : I_j \leq I_{\max_j}, \omega_{0j} \geq \omega_{\max}, m_{mj} \leq m_{m_{\max}}\}. \quad (27)$$

257 Like in the propeller's case, various selection criteria could be used to choose the motor. In
 258 the simple example for $n_o = 1$ it could be the lowest electrical power

$$259 \quad m_{\text{selected}} := \arg \min_{\mathbf{m}_j \in \mathcal{M}_p} P_{ej}^{(1)}. \quad (28)$$

260 3.1.3 ESC and battery sizing

261 The Electronic Speed Controller is sized mainly in regards to the maximum current it can handle.
 262 As it is assumed that the multicopter will never need more thrust than achieved at WOT operating
 263 point, the current should also not go over the calculated value. Therefore, it can be said that

$$264 \quad I_{\text{ESC}} = I_{\text{selected}}^{(2)} \quad (29)$$

265 where I_{ESC} is the rated (maximal) ESC current and $I_{\text{selected}}^{(2)}$ is the motor current at WOT operating
 266 point.

267 A substantial part of battery specification needs to be provided by the user to realise flight
 268 time estimation as described in the Subsection 3.2. However, the methodology allows to complete
 269 the battery specification by sizing the C-rating parameter

$$270 \quad r_C = \frac{I_{\text{ESC}} \times n_{\text{rot}}}{C} \quad (30)$$

271 where r_C is the minimal required battery C-rating and C is the battery capacity.

272 The whole actuating system sizing methodology is depicted by the data flow chart shown in
 273 Figure 6. It shows the dependence of motor sizing on propeller specification and ESC and battery
 274 sizing on motor specification. The light cyan blocks correspond to the methodology stages, the dark
 275 blue blocks show requirements and constraints and the orange ellipses signify points of database
 276 access. The output data in green ellipses includes specification parameters for sizing all of the
 277 major components of the propulsion system (namely propeller, motor, ESC and battery) and the
 278 calculated propeller and motor operating points that can be used for calculating additional data, such
 279 as estimated flight time. The data corresponding to each of the outputs can be found in Table 2.

280 In figure 6 a substantial impact of estimated total drone weight can be also seen - it is used to
 281 calculate required thrust T_r that plays a key role in selecting the propeller, and consequently the

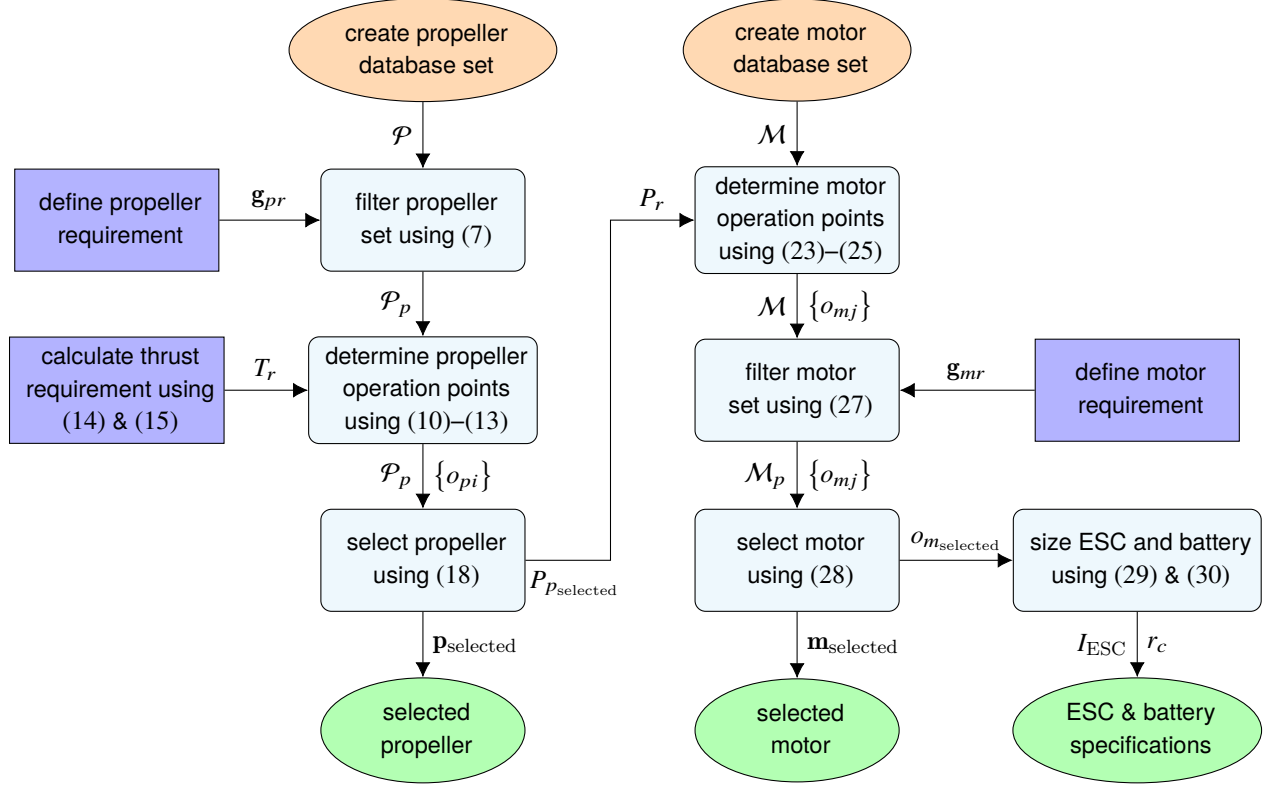


Figure 6: Actuating system sizing methodology information flow diagram.

Table 2: Data contained in sizing methodology outputs

Output name	Data contained
Propeller specification	name; diameter d ; pitch θ_p ; series s_n
Motor specification	name; KV rating; rated speed $\omega_{\text{selected}}^{(2)}$; rated torque $\tau_{\text{selected}}^{(2)}$; rated mech. power $P_{m_{\text{selected}}}^{(2)}$; rated el. power $P_{e_{\text{selected}}}^{(2)}$; rated efficiency $\eta_{\text{selected}}^{(2)}$; nominal voltage V
ESC specification	maximum current I_{ESC}
Battery specification	cell number n_C ; minimum C rating r_C ; capacity C

282 motor. Due to the discrete nature of propeller and motor parameters, the relationship is highly
 283 nonlinear, so it needs to be analysed numerically. However, it is easy to implement the methodology
 284 in a loop to plot the characteristics of flight time versus weight, which may be used in a payload
 285 sizing application.

286 3.2 Power system

287 The power system section of the methodology focuses on flight time estimation by modelling the
 288 battery. The model is based on the iterative approach presented by Traub [11]. It features 2 important

289 phenomena - decrease of capacity with the increase of current and drop in voltage due to discharge.
 290 Additionally, the power demand can be varied throughout the simulation, however, in the base
 291 version of the methodology this is not used, as the operating points are constant. A block diagram
 292 of the calculations for one operating point can be seen in Figure 7.

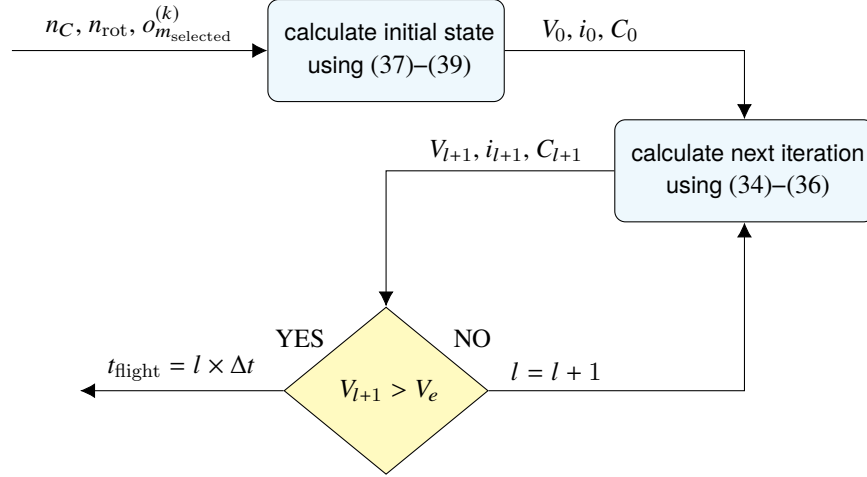


Figure 7: Power system calculation flowchart for k th operating point.

293 Modelling of the battery capacity varying with drawn current is done through modified
 294 Peukert's equation in the form of:

$$295 \quad t = \frac{Rt}{i^n} \left(\frac{C}{Rt} \right)^n \quad (31)$$

296 where Rt is battery hour rating (1 hour in case of small packs) and n is Peukert's constant (1.3 for
 297 LiPo) dependent on battery type and temperature.

298 Measuring battery voltage is one of the main ways of measuring remaining charge in-flight.
 299 Typically, Lithium Polymer (LiPo) cells used in drones have 4.2 V when at full charge and drop
 300 to 3.7 V when at 20% charge. The voltage drop curve is nonlinear, but for the model it has been
 301 linearized and is expressed through

$$302 \quad V(t) = V_0 - k_1 [C_0 - C(t)], \quad (32)$$

$$303 \quad k_1 = \frac{4.2V - 3.7V}{DoD \times C_0 \times n_C} \quad (33)$$

304 where V_0 is the initial voltage, k_1 is the voltage drop coefficient, C_0 is the initial battery capacity,
 305 DoD is the maximal Depth of Discharge and n_C is the number of battery cells. Based on Traub [11]
 306 the battery model can be defined with a set of iterative equations

$$307 \quad V_{l+1} = V_0 - k_1 [C_0 - C_l], \quad (34)$$

$$308 \quad i_{l+1} = \frac{P_e}{V_{l+1}}, \quad (35)$$

$$309 \quad C_{l+1} = i_{l+1}^{1-n} Rt^{1-n} C^n - \sum_{m=1}^{l+1} i_m \Delta t \quad (36)$$

310 with the initial state defined as

$$311 \quad V_0 = 4.2V \times n_C, \quad (37)$$

$$312 \quad i_0 = \frac{P_e}{V_0}, \quad (38)$$

$$313 \quad C_0 = i_0^{1-n} R t^{1-n} C^n. \quad (39)$$

314 The information flow in the model is visualized in Figure 7.

315 As time passes, the voltage decreases, therefore increasing current draw to achieve the same
 316 power, and consecutively decreasing available battery capacity due to Peukert's effect, as can be
 317 seen in Figure 8. The simulation is stopped when voltage reaches

$$318 \quad V_e = 3.7V \times n_C \quad (40)$$

319 or when capacity reaches 20% of initial capacity (only works when power drawn is constant). The
 320 output is simply the simulation time, calculated as the product of the time step value and the number
 321 of iterations.

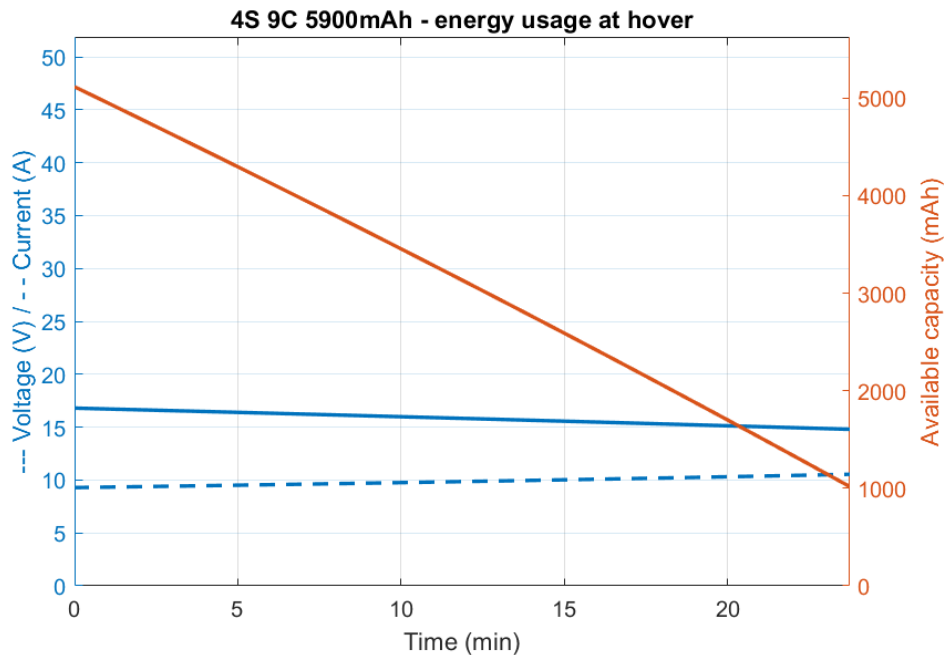


Figure 8: Example battery behaviour during hover.

322 4 Example results

323 The methodology presented has been implemented as a MATLAB script. This allows to easily process
 324 large quantities of data from propeller and motor databases and to plot component characteristics on
 325 every stage of the selection process.

326 In this example, performance data published by APC Propellers [12] will be used for the
 327 propeller database. It contains static and dynamic performance obtained through analytical methods
 328 of all products currently manufactured by the company. Due to the reliance on external computer
 329 software, airfoil drag (and consequently, torque) may be under-predicted at low speeds. Additionally,
 330 wind tunnel measurements of selected propellers [13] show over-prediction of thrust coefficient (and
 331 consequently, thrust) of around 12% on average across all tested propellers. Detailed results are
 332 shown in Table 3 and in Figure 9. Therefore, an easily adjustable parameter called *Safety Factor*
 333 (*SF*) was introduced that increases required power at the WOT operating point to reduce the impact
 334 of mentioned inaccuracies and guarantee that the chosen motor will be able to reach the expected
 335 speed

$$336 \quad I_j^{(2)} = P_m^{-1}(P_r \times SF), \quad (41)$$

$$337 \quad \eta_j^{(2)} = \eta(P_r \times SF, P_{ej}). \quad (42)$$

338 There is no need to include *Safety Factor* in the ESC sizing, as the WOT operating point at which it
 339 is sized, in typical operating conditions, is achieved only for a few seconds at a time, not enough to
 340 damage the unit. The inclusion of the *Safety Factor* parameter in the battery sizing is recommended,
 341 as LiPo batteries are prone to ageing, which increases their internal resistance. Hence, with time at
 342 high currents more and more heat is generated, eventually leading to battery damage. What is more,
 343 cheap batteries are known for parameters varying between each unit, further justifying the need for
 344 an additional safety measure. Therefore, Equation (30) becomes

$$345 \quad r_C = \frac{I_{ESC} \times n_{rot} \times SF}{C}. \quad (43)$$

Table 3: Errors between measured and simulated propeller characteristics - thrust coefficient (C_T) and power coefficient (C_P).

Mean C_T error	-0.0121
Mean relative C_T error	-12.6306%
Mean std. deviation of C_T	0.0051
Mean C_P error	0.0059
Mean relative C_P error	2.4816%
Mean std. deviation of C_P	0.0022

346 For the motor database, a database bundled with Drive Calculator [2] software was used. It is
 347 based on measurements done and uploaded by its users, so it is impossible to accurately measure the
 348 discrepancies with real products, but they are estimated to be around 5-10% overall. However, a
 349 significant inaccuracy is introduced with the simplified motor model used to calculate characteristics
 350 based on scarce data. The model, applicable both to BLDC and DC motors, considers only two
 351 sources of losses: copper losses, calculated using winding resistance

$$352 \quad P_{Cu} = R_m I_{motor}^2 \quad (44)$$

353 and iron losses, calculated using no-load current

$$354 \quad P_{iron} = V \times I_0 \quad (45)$$

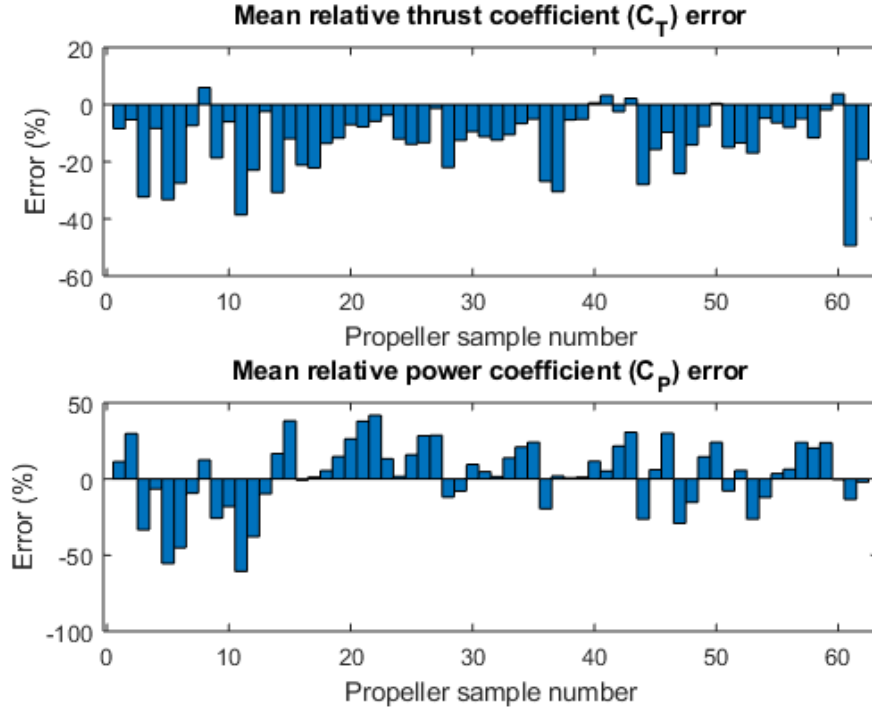


Figure 9: Relative errors between measured and simulated propeller coefficients.

355 where P_{Cu} are copper losses, R_m is the windings resistance, I_{motor} is the current delivered to motor
 356 windings, P_{iron} are iron losses, V is the nominal voltage and I_0 is the no-load current. As the
 357 no-load measurement is usually done through an ESC, the iron losses also incorporate losses from
 358 the controller. The model, based on [14], is calculated as follows:

$$359 \quad P_{prop} = \tau_{prop} \times \omega_{prop} \times SF, \quad (46)$$

$$360 \quad I_{motor} = \frac{V - \sqrt{V^2 - 4R_m(P_{iron} + P_{prop})}}{2R_m}, \quad (47)$$

$$361 \quad P_{motor} = V \times I_{motor}, \quad (48)$$

$$362 \quad \eta_{motor} = \frac{P_{prop}}{P_{motor}} \times 100\% \quad (49)$$

363 where P_{prop} - is the power delivered to the propeller, τ_{prop} is the propeller torque, ω_{prop} is the
 364 propeller speed, P_{motor} is the motor electrical power and η_{motor} is the motor efficiency.

365 To demonstrate the capabilities of the methodology a set of example results is presented
 366 for a low-weight drone. The results are validated against a similar commercial product. Based
 367 on the findings, a hypothetical usage of the methodology for sizing of Personal Air Vehicles is
 368 demonstrated.

369 4.1 Small drone

370 For the ease of validation, the input parameters of the methodology were set to match those of the DJI
 371 Phantom 4 Pro V2.0, as indicated in Table 4. This enables easy comparison of the vehicle's published

372 specification [15] with the sizing method's results in terms of flight time and propeller dimensions, as
 373 the manufacturer does not provide motor data. It should be noted here that the Phantom 4 uses LiHV
 374 (High Voltage LiPo) batteries rated at 3.8 V per cell, however in the calculations the more popular
 375 LiPo batteries, rated at 3.7 V per cell, are used. Additionally, V2.0 uses FOC-enabled drivers, which
 376 generate sinusoidal signals instead of the usual trapezoidal. However, the manufacturer advertises it
 377 as a means to reduce noise instead of improving performance, so it can be assumed that in this case
 378 the difference can be neglected.

Table 4: Basic DJI Phantom 4 V2.0 parameters.

Number of rotors	4
Diagonal size	350 mm
Total weight	1375 g
Battery weight	468 g
Battery capacity	5870 mAh
Battery nominal voltage	15.2 V
Battery type	LiHV 4S
Propeller diameter	9 inch
Propeller pitch	5.5 inch

Table 5: Additional methodology parameters used in small drone sizing.

Thrust-to-weight ratio r_r	3
Min. propeller diameter d_{\min}	8 inch
Max. propeller diameter d_{\max}	9 inch
Safety Factor SF	1.05
Preferred propeller series \mathcal{S}_{n_r}	MR, E, E-3, E-4
Max. propeller mass m_{p_r}	24 g
Max. motor mass m_{m_r}	100 g

379 The MATLAB script has been run considering 2 operating points: hover and WOT. The goal
 380 was to reduce energy usage at hover, as the platform's main purpose is photography. For the thrust
 381 the unit of gram-force (gf), which corresponds to the force acting on 1 gram of mass in a standard
 382 gravitational field, is used due to intuitiveness in this application. Additional sizing parameters are
 383 listed in Table 5. The results are below:

384 **Results** For a 4-rotor drone with estimated AUM of 1375 g:

- 385 • APC 9x4.5E propeller should be chosen for the highest specific thrust of 8.81 gf/W per motor
 386 at hover.
- 387 • Flyduino X2208 (1160 KV) motor should be selected with 0.15 Nm torque at maximum speed
 388 of 9600 RPM.
- 389 • The motor uses 39 W of electrical power at hover and 174 W of electrical power at WOT.

- The drive should be controlled by a 12 A ESC per motor.
- The whole system should be powered by a 4S 9C LiPo battery of 5870 mAh.
- Hovering flight requires 31 W of mechanical power (0.05 Nm at 5600 RPM) to achieve 1375 gf of total thrust.
- WOT flight requires 147 W of mechanical power (0.14 Nm at 9600 RPM) to achieve 4125 gf of total thrust.
- This configuration should achieve around 24 min of hover and around 3 min of flight at WOT.

As can be seen, both the propeller and the motor were successfully selected and the estimated flight time has been calculated. The propeller is of lower pitch than in the reference drone, which might be explained by the unavailability of 9x5.5 propellers in APC range, and 9x6 being too power-consuming. Especially interesting is the choice of E-series (electric airplanes) propeller over MR-series (multirotors), which can be influenced by numerical errors due to interpolation, specifically at low speeds required for hovering. Comparison of power characteristics of propellers considered in this example can be seen in Figure 10.

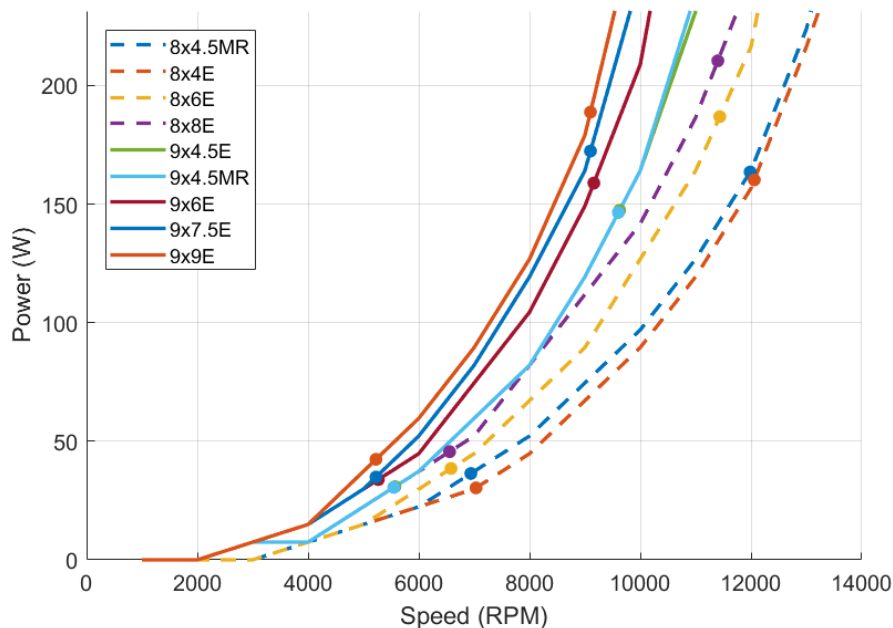


Figure 10: Comparison of power-speed characteristics of 8 and 9 inch propellers.

Flyduino X2208 has 22 mm stator diameter and 8 mm height, which is typically used in 5-7 inch builds [10], which results in usually high current required to achieve hover. However, 1160 KV (1100 KV according to manufacturer [16]) version chosen here has peak efficiency pushed towards a lower current than the typical 2000 KV version. The combination of those factors grants the hover operating point close to peak efficiency, therefore increasing flight time. This is illustrated in Figure 11.

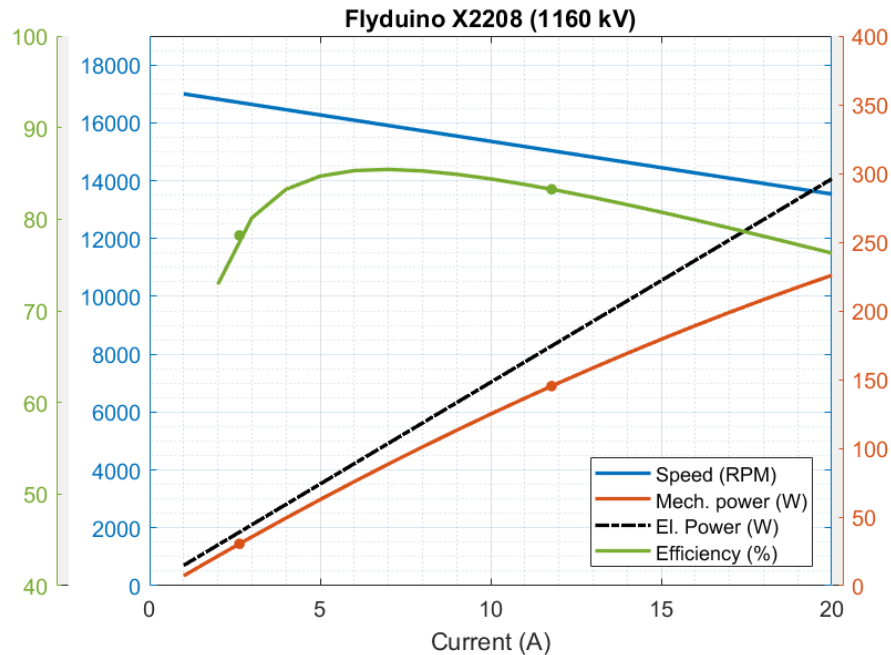


Figure 11: Simulated operating characteristics of Flyduino X2208 brushless motor.

410 The calculated flight time seems to be in line with the achievements of the reference drone.
 411 Maximum flight time stated by the manufacturer is 30 min ([15]), but it was probably measured
 412 in flight at best endurance speed, which uses slightly less power than in hover ([17]) due to the
 413 reduction of the induced drag. Therefore, it can be assumed that the maximum hover time will be
 414 close to the 24 min calculated, which seems to be confirmed by independent tests achieving 23-26
 415 min of hover [18], [19]. However, as the calculations do not include dynamic effects of flight, the
 416 prediction accuracy for the WOT operating point is considerably lower. Furthermore, that point
 417 is set arbitrarily based on thrust-to-weight ratio, and is rarely measured in real operation, so no
 418 validation could be performed.

419 The reference drone is a commercially popular product, therefore it can be assumed that its
 420 performance is close to optimal for its given weight and application (aerial photography). Therefore,
 421 achieving results of similar value to the reference may indicate that the chosen configuration has
 422 performance close to optimal. Considering the accuracy of results, the assumptions and estimations
 423 used and the low computational cost, methodology performance can be considered satisfactory for
 424 applications in other research projects and on its own.

425 4.2 Personal Air Vehicle

426 Current implementation of methodology as a MATLAB script does not allow to size heavy
 427 platforms, such as PAV, due to the lack of sufficiently large propellers in the database. However, the
 428 methodology can be implemented with different databases and even modified to help with the design
 429 of components: propeller specification provides enough data for pre-sizing of an electric motor, and
 430 thrust requirements along with size and weight constraints can be used as input in propeller design.
 431 Additionally, using only scarce data, a flight time estimation can be performed to validate the design

432 of components. This is an especially important feature, as the methodology has been designed with
 433 the ability to be used inside another algorithm to further enhance the optimisation process. That
 434 way questions, such as rotor number, propeller size or maximum payload, can be answered. This is
 435 especially important for PAV, where the mass constraint is very tight because of the payload in the
 436 form of a passenger. Table 6 outlines example uses of the methodology in scenarios with different
 437 data available.

Table 6: Uses of sizing methodology based on data available.

Propeller data	Motor data	Example uses
available	available	complete sizing of multirotor propulsion system; flight time estimation; optimisation of flight time
available	not available	propeller sizing; preliminary motor design
not available	available	battery and ESC sizing; flight time estimation
not available	not available	–

438 **5 Conclusion**

439 The methodology presented in this paper answers the need to have an automated process of selecting
 440 multirotor components using a simple input of estimated drone weight. Validation was performed
 441 using data from a commercially available multirotor (DJI Phantom 4 V2.0), which shows that the
 442 obtained results are in accordance with manufacturer data and independent tests.

443 The simplicity and open-loop approach are also the limitations of this methodology. The
 444 use of static model does not provide enough information to estimate the acceleration, turn speed or
 445 performance in wind conditions. However, the inclusion of a dynamic model would require the
 446 bandwidth limitations of the actuators to be considered. This would overly increase the complexity
 447 of the methodology and would demand much more input data, thus limiting the usability.

448 Although there are no conceptual constraints preventing the use of the methodology for sizing
 449 large passenger multirotors, considerable limitations are introduced by the databases used, which
 450 rarely provide data on large propellers in the 50-60 inch range and motors able to support them.
 451 However, it is assumed, that certain elements of the methodology, such as flight time estimation
 452 based on limited data, can be useful in the process of PAV design. Unfortunately, one of the most
 453 important disadvantages of this methodology is its low, hard to estimate, accuracy. Great care was
 454 taken to make the results as close to reality as possible, but due to assumptions made for the sake of
 455 simplicity and speed, such as the use of thrust-to-weight ratio instead of calculation of maximum
 456 required thrust, the accuracy of calculations is impossible to measure. If needed, it can be enhanced,
 457 for example by improving motor model or using databases with only measured data, but it is advised
 458 against relying on the results in safety-critical applications.

459 **Data Availability**

460 The MATLAB code used to support the findings of this study have been deposited in the GitHub
 461 repository (<https://github.com/mbiczyski/Multirotor-Sizing-Methodology>).

462 APC propeller performance data used to support this study is available at <https://www.apcprop.com/technical->
463 [information/performance-data/](https://www.apcprop.com/technical-information/performance-data/). These datasets are cited at relevant places within the text as reference
464 [12].

465 Previously reported propeller experimental performance data were used to support this study and
466 are available at <http://m-selig.ae.illinois.edu/props/propDB.html>. These prior studies (and datasets)
467 are cited at relevant places within the text as reference [14].

468 Motor performance data used to support this study is available at <http://www.drivecalc.de/>. These
469 datasets are cited at relevant places within the text as reference [3].

470 **Conflicts of Interest**

471 The authors declare that there is no conflict of interest regarding the publication of this paper.

472 **Funding Statement**

473 Research and publication of the article was funded by ESTACA, France, and Cranfield University,
474 UK.

References

- 476 [1] G. Szafranski, R. Czyba, and M. Blachuta, "Modeling and identification of electric propulsion
477 system for multicopter unmanned aerial vehicle design," in *2014 International Conference
478 on Unmanned Aircraft Systems, ICUAS 2014 - Conference Proceedings*, 2014, pp. 470–476,
479 ISBN: 9781479923762. DOI: 10.1109/ICUAS.2014.6842287.
- 480 [2] C. Persson, *Drive Calculator*. [Online]. Available: <http://www.drivecalc.de/>
481 (Accessed: 2019-05-24).
- 482 [3] Solution for All Markus Müller, *eCalc - the most reliable electric Motor Calculator on the Web
483 for RC Pilots*. [Online]. Available: <https://www.ecalc.ch/> (Accessed: 2019-06-11).
- 484 [4] P. Basset, A. Tremolet, and T. Lefebvre, "Rotary Wing UAV pre-sizing : Past and Present
485 Methodological Approaches at Onera," *Aerospace Lab*, no. 8, pp. 1–12, 2014. DOI: 10.
486 12762/2014.AL08-10.
- 487 [5] M. Gatti and F. Giuliotti, "Preliminary Design Analysis Methodology for Electric Multicopter,"
488 *IFAC Proceedings Volumes*, vol. 46, no. 30, pp. 58–63, 2013, ISSN: 14746670. DOI: 10.3182/
489 20131120-3-FR-4045.00038.
- 490 [6] M. Gatti, "Complete Preliminary Design Methodology for Electric Multicopter," *Journal of
491 Aerospace Engineering*, vol. 30, no. 5, Sep. 2017, ISSN: 0893-1321. DOI: 10.1061/(ASCE)
492 AS.1943-5525.0000752.
- 493 [7] M. Kim, H. Joo, and B. Jang, "Conceptual multicopter sizing and performance analysis
494 via component database," in *2017 Ninth International Conference on Ubiquitous and
495 Future Networks (ICUFN)*, IEEE, Jul. 2017, pp. 105–109, ISBN: 978-1-5090-4749-9. DOI:
496 10.1109/ICUFN.2017.7993756.
- 497 [8] J. M. Miller, "Energy storage technologies," in *Propulsion Systems for Hybrid Vehicles*,
498 Institution of Engineering and Technology, 2010, ch. 10, pp. 439–522, ISBN: 9781466585096.
499 DOI: 10.1049/PBRN007E{_}ch10.
- 500 [9] Half Chrome Drones, *Drone Thrust Testing*. [Online]. Available: [https://www.halfchrome.
501 com/drone-thrust-testing/](https://www.halfchrome.com/drone-thrust-testing/) (Accessed: 2019-05-29).
- 502 [10] O. Liang, *How to choose Motor for Racing Drone & Quadcopter*. [Online]. Available: [https:
503 //oscarliang.com/quadcopter-motor-propeller/](https://oscarliang.com/quadcopter-motor-propeller/) (Accessed: 2019-05-27).
- 504 [11] L. W. Traub, "Range and Endurance Estimates for Battery-Powered Aircraft," *Journal of
505 Aircraft*, vol. 48, no. 2, pp. 703–707, Mar. 2011, ISSN: 0021-8669. DOI: 10.2514/1.C031027.
- 506 [12] APC Propellers, *Performance Data*. [Online]. Available: [https://www.apcprop.com/
507 technical-information/performance-data/](https://www.apcprop.com/technical-information/performance-data/) (Accessed: 2019-05-24).
- 508 [13] J. Brandt, R. Deters, G. Ananda, and M. Selig, *UIUC Propeller Database*. [Online]. Available:
509 <http://m-selig.ae.illinois.edu/props/propDB.html> (Accessed: 2019-05-
510 21).
- 511 [14] Radio Control Info, *Brushless Motor Efficiency and Constants*. [Online]. Available: [http:
512 //www.radiocontrolinfo.com/brushless-motor-efficiency/](http://www.radiocontrolinfo.com/brushless-motor-efficiency/) (Accessed: 2019-
513 06-18).

- 514 [15] DJI, *DJI Phantom 4 Pro V2.0*. [Online]. Available: [https://www.dji.com/uk/phantom-](https://www.dji.com/uk/phantom-4-pro-v2/info/)
515 [4-pro-v2/info/](https://www.dji.com/uk/phantom-4-pro-v2/info/) (Accessed:2019-05-24).
- 516 [16] Flyduino, *Flyduino X2208v2 light edition 1100KV Brushless Outrunner Motor CCW Version*.
517 [Online]. Available: [https://www.flyduino.net/en_US/shop/product/pr1934-](https://www.flyduino.net/en_US/shop/product/pr1934-flyduino-x2208v2-light-edition-1100kv-brushless-outrunner-motor-ccw-version-2713/)
518 [flyduino-x2208v2-light-edition-1100kv-brushless-outrunner-motor-ccw-](https://www.flyduino.net/en_US/shop/product/pr1934-flyduino-x2208v2-light-edition-1100kv-brushless-outrunner-motor-ccw-version-2713/)
519 [version-2713/](https://www.flyduino.net/en_US/shop/product/pr1934-flyduino-x2208v2-light-edition-1100kv-brushless-outrunner-motor-ccw-version-2713/) (Accessed:2019-05-27).
- 520 [17] C. Di Franco and G. Buttazzo, “Energy-Aware Coverage Path Planning of UAVs,” in *2015*
521 *IEEE International Conference on Autonomous Robot Systems and Competitions*, IEEE, Apr.
522 2015, pp. 111–117, ISBN: 978-1-4673-6991-6. DOI: 10.1109/ICARSC.2015.17. [Online].
523 Available: <http://ieeexplore.ieee.org/document/7101619/>.
- 524 [18] T. Luna, *DJI Mavic 2 Pro vs. Phantom 4 Pro v2.0!* 2018. [Online]. Available: [https:](https://www.wetalkuav.com/dji-mavic-2-pro-vs-phantom-4-pro-v2-0/)
525 [//www.wetalkuav.com/dji-mavic-2-pro-vs-phantom-4-pro-v2-0/](https://www.wetalkuav.com/dji-mavic-2-pro-vs-phantom-4-pro-v2-0/) (Accessed:
526 2019-05-24).
- 527 [19] K. Smith, *DJI Mavic Pro VS Phantom 4 Pro V2.0 : Which Drone Is Better?* 2018. [Online].
528 Available: [https://myfirstdrone.com/blog/dji-mavic-pro-vs-phantom-4-pro-](https://myfirstdrone.com/blog/dji-mavic-pro-vs-phantom-4-pro-drone-better/)
529 [drone-better/](https://myfirstdrone.com/blog/dji-mavic-pro-vs-phantom-4-pro-drone-better/) (Accessed:2019-05-24).